European Journal of Pharmaceutical Sciences 123 (2018) 228–240

Contents lists available at ScienceDirect

European Journal of Pharmaceutical Sciences

journal homepage: www.elsevier.com/locate/ejps

Niosomes decorated with dual ligands targeting brain endothelial transporters increase cargo penetration across the blood-brain barrier

Mária Mészáros[a,b], Gergő Porkoláb[a,c], Lóránd Kiss[a,1], Ana-Maria Pilbat[d], Zoltán Kóta[a], Zoltán Kupihár[e], Albert Kéri[f], Gábor Galbács[f], László Siklós[a], András Tóth[a,g], Lívia Fülöp[e], Mária Csete[h], Áron Sipos[a], Petra Hülper[i,2], Péter Sipos[j], Tibor Páli[a], Gábor Rákhely[a,g], Piroska Szabó-Révész[j], Mária A. Deli[a,*], Szilvia Veszelka[a,*]

[a] Institute of Biophysics, Biological Research Centre of the Hungarian Academy of Sciences, Temesvári krt. 62, H-6726 Szeged, Hungary
[b] Doctoral School in Theoretical Medicine, Faculty of Medicine, University of Szeged, H-6720 Szeged, Hungary
[c] Foundation for the Future of Biomedical Sciences in Szeged, Pálfy u. 52/d, H-6725 Szeged, Hungary
[d] Institute of Biochemistry, Biological Research Centre of the Hungarian Academy of Sciences, Temesvári krt. 62, H-6726 Szeged, Hungary
[e] Department of Medical Chemistry, Faculty of Medicine, University of Szeged, Dóm tér 8, H-6720 Szeged, Hungary
[f] Department of Inorganic and Analytical Chemistry, Faculty of Science and Informatics, University of Szeged, Dóm tér 7, H-6720 Szeged, Hungary
[g] Department of Biotechnology, Faculty of Science and Informatics, University of Szeged, Szeged, Hungary, Közép fasor 52, H-6726 Szeged, Hungary
[h] Department of Optics and Quantum Electronics, Faculty of Science and Informatics, University of Szeged, Dóm tér 9, H-6720 Szeged, Hungary
[i] Department of Pediatrics I, University Medical Center Göttingen, Robert-Koch-Straße 40, 37075 Göttingen, Germany
[j] Institute of Pharmaceutical Technology and Regulatory Affairs, Faculty of Pharmacy, University of Szeged, Eötvös u. 6, H-6720 Szeged, Hungary

ARTICLE INFO

Keywords:
Blood-brain barrier
Brain endothelial cell
Drug targeting
Dual-ligand
Nanoparticle
Niosome
Solute carriers

ABSTRACT

Nanoparticles targeting transporters of the blood-brain barrier (BBB) are promising candidates to increase the brain penetration of biopharmacons. Solute carriers (SLC) are expressed at high levels in brain endothelial cells and show a specific pattern at the BBB. The aim of our study was to test glutathione and ligands of SLC transporters as single or dual BBB targeting molecules for nanovesicles. High mRNA expression levels for hexose and neutral amino acid transporting SLCs were found in isolated rat brain microvessels and our rat primary cell based co-culture BBB model. Niosomes were derivatized with glutathione and SLC ligands glucopyranose and alanine. Serum albumin complexed with Evans blue (67 kDa), which has a very low BBB penetration, was selected as a cargo. The presence of targeting ligands on niosomes, especially dual labeling, increased the uptake of the cargo molecule in cultured brain endothelial cells. This cellular uptake was temperature dependent and could be decreased with a metabolic inhibitor and endocytosis blockers filipin and cytochalasin D. Making the negative surface charge of brain endothelial cells more positive with a cationic lipid or digesting the glycocalyx with neuraminidase elevated the uptake of the cargo after treatment with targeted nanocarriers. Treatment with niosomes increased plasma membrane fluidity, suggesting the fusion of nanovesicles with endothelial cell membranes. Targeting ligands elevated the permeability of the cargo across the BBB in the culture model and in mice, and dual-ligand decoration of niosomes was more effective than single ligand labeling. Our data indicate that dual labeling with ligands of multiple SLC transporters can potentially be exploited for BBB targeting of nanoparticles.

1. Introduction

The blood-brain barrier (BBB) restricts the entry of the potential neuropharmaceuticals, especially biopharmacons, like nucleic acids, peptide or protein drugs into the central nervous system (CNS). Although it is generally assumed that small molecule drugs can cross the BBB, actually, only about a small fraction of them is able to enter the brain parenchyma (Pardridge, 2015). Several clinical trials ended with failure because of the low penetration of the biologic drugs across the BBB (Pardridge, 2016). Strategies to solve this problem can be

* Corresponding authors.
E-mail addresses: deli.maria@brc.mta.hu (M.A. Deli), veszelka.szilvia@brc.mta.hu (S. Veszelka).
[1] Present affiliation: Department of Pathophysiology, University of Szeged, Semmelweis u. 1, H-6701 Szeged, Hungary.
[2] Present affiliation: Department of Neuroscience, Carl von Ossietzky University, 26,111, Oldenburg, Germany.

https://doi.org/10.1016/j.ejps.2018.07.042
Received 20 March 2018; Received in revised form 13 July 2018; Accepted 19 July 2018
Available online 20 July 2018
0928-0987/

classified into three major groups, namely (i) circumvention of the BBB, (ii) modification of the BBB functions, (iii) modification of the molecules (Deli, 2011). Invasive drug delivery strategies, like intraventricular or intrathecal drug administration are successful in circumventing the BBB, however limitations, such as potential infectious risks must be considered. The non-invasive alternative nasal pathway is also being investigated for transport of molecules to the brain (Horvát et al., 2009; Sipos et al., 2010) but the major drawbacks of this method are the very low amount of molecules transported to the brain and limited distribution. Modification of BBB functions with transient increase of brain endothelial permeability pathways (Hülper et al., 2013; Walter et al., 2015) could potentially increase CNS drug delivery if problems with safety, reversibility, systemic and CNS side-effects will be solved in the future. Medicinal chemistry uses several methods to enhance brain delivery of molecules by changing their physico-chemical properties, including techniques to increase the lipid solubility or cationic charge of molecules. While high lipid solubility can augment the transport of a given drug across the BBB it can also enhance its uptake by peripheral tissues and also sequestration in the capillary bed resulting in decreased concentration in blood and in the CNS (Banks, 2009). Therefore new approaches are needed to improve the brain delivery of drugs.

Nanosized drug carriers, or nanoparticles (NP) are in the focus of research efforts to develop successful drug delivery systems for the CNS (Masserini, 2013; Saraiva et al., 2016; Zhou et al., 2018). Vesicular NPs are especially versatile, because they can accomodate drug cargo with different properties. The non-ionic surfactant based vesicular nanocarriers, niosomes, have several favorable properties such as good biocompatibility and biodegradability, non-immunogenicity, and physical stability. Niosomes are also able to accumulate both water and lipid soluble drugs and control their release (Abdelkader et al., 2014). Another advantage of nanovesicles is that they increase the penetration of drugs across biological barriers and reduce their toxic side effects due to the encapsulation process (Masserini, 2013). However, the encapsulation of drugs in NPs alone is not enough for the successful delivery of drugs to the CNS, specific targeting is needed to elevate the BBB specific uptake and permeability of drugs (Kreuter, 2014). Various essential influx transport systems are expressed on the cerebral endothelium, which have physiological role in the delivery of nutrients and can be potentially exploited to shuttle nanocarriers to the brain, including receptor mediated endocytosis, adsorptive mediated endocytosis and carrier mediated transport systems (Abbott, 2013; Campos-Bedolla et al., 2014). The receptor mediated transport pathway and the ligands of BBB receptors are widely investigated to deliver fusion peptides or NPs to the brain (Pardridge, 2012; Johnsen and Moos, 2016).

Solute carriers (SLC) compose a large family of transporters at the BBB delivering nutrients (Enerson and Drewes, 2006; Campos-Bedolla et al., 2014). Several clinically used drugs cross the endothelial cells of brain capillaries *via* SLCs. The most well known drug to treat Parkinson's disease, L-DOPA, enters the brain *via* the LAT1/SLC7A5 transporter (Pardridge, 2015). SLC transporters are actively investigated as drug targets and the number of drug candidates developed for SLCs and reaching clinical trials increases (Rask-Andersen et al., 2013). However this pathway is not fully exploited for drug delivery (César-Razquin et al., 2015), especially for targeted NPs.

Among the SLC transporters, the expression level of glucose transporter GLUT1 (SLC2A1) is the highest at the BBB, but other members of the SLC2A family are also present (Campos-Bedolla et al., 2014; Enerson and Drewes, 2006). Glucose analogs have a potential to be efficient and selective targeting ligands for both vesicular and gold nanocarriers to cross the BBB (Dufes et al., 2004; Gromnicova et al., 2013). The number and expression level of SLCs transporting amino acids across the BBB are also high (Enerson and Drewes, 2006; Shawahna et al., 2011). Neutral amino acids, like alanine, serine and cysteine, are transported by carriers belonging to the SLC38A sodium coupled amino acid transporter family (SLC38A1, SLC38A2, SLC38A5) and the SLC1A neutral amino acid transporters (ASCT1/SLC1A4, ASCT2/SLC1A5) (Campos-Bedolla et al., 2014). These neutral amino acids could be also considered as targeting molecules, but have not been used for decorating nanocarriers yet. SLCs also transport vitamins to brain (Campos-Bedolla et al., 2014). The Na^+-dependent multivitamin transporter SLC5A6 mediates the uptake of biotin in brain endothelial cells (Uchida et al., 2015). We were the first to demonstrate that biotin as a targeting ligand significantly elevated the uptake and permeability of solid NPs in cultured human brain endothelial cells as compared to non-targeted NPs (Veszelka et al., 2017). Since the expression pattern of SLCs is specific for the BBB, our hypothesis was that labeling vesicular NPs with two different SLC ligands (dual targeting) will increase the brain endothelial uptake of the cargo and its permeability across the BBB as compared to a single ligand.

One of the most successful targeting ligands of NPs to cross the BBB is the tripeptide glutathione. There is an active glutathione transport across the BBB, but the transporter(s) were not yet identified (Gaillard, 2016). Nevertheless glutathione, as a targeting ligand, increased drug delivery to brain by NPs in several studies (Birngruber et al., 2014; Lindqvist et al., 2016). The group of Gaillard established the efficacy of glutathione targeted liposomal doxorubicin in a mouse glioma model (Gaillard et al., 2014) and these NPs were also investigated in clinical trials (Gaillard, 2016).

The aim of our study was to test glucopyranose and alanine, ligands of SLC transporters, as single or dual BBB targeting molecules for nanovesicles loaded with a large biomolecule, serum albumin, as cargo. Glutathione was used as a reference BBB targeting ligand. We characterized the properties of the different niosomes and investigated their effects on viability, cellular uptake and permeability of the cargo using a BBB culture model. The mechanism of the cellular uptake process and the role of the brain endothelial surface charge were also studied. Single and dual-targeted niosomes were also examined in mice using optical imaging.

2. Materials and methods

2.1. Animals

Animal studies were performed following the regulations of the 1998. XXVIII. Hungarian law and the EU Directive 2010/63/EU about animal protection and welfare. Approval for animal studies was obtained from the local animal health authority, the Governmental Office for Csongrád County, Directorate of Food Chain Safety and Animal Health (Permit numbers: XVI./03835/001/2006, XVI./834/2012). For the *in vivo* experiments ten week old male CD1-Foxn1nu nude mice (Charles River Laboratories, Wilmington, MA, USA) were used. For the *in vitro* primary cell isolations, brain tissues were obtained from 3-week-old and newborn outbred Wistar rats (Harlan Laboratories, United Kingdom) of both sexes. Animals were fed on standard rodent chow and water *ad libitum* and kept under a 12 h light/dark cycle in the conventional animal house of the Biological Research Centre. During the experiments, all efforts were made to minimize animal suffering and pain.

2.2. Materials

All reagents were purchased from Sigma-Aldrich Kft., Hungary (part of Merck Life Science), except for those specifically mentioned.

2.3. Synthesis of targeted ligands for niosomes

For the synthesis of DSPE-PEG-glutathione, 13.5 mg glutathione (0.044 mM) was reacted with 100 mg DSPE-PEG-maleimide (0.035 mM) (N-[(3-Maleimide-1-oxopropyl) aminopropyl polyethyleneglycol-carbamyl] distearoylphosphatidyl-ethanolamine,

SUNBRIGHT® DSPE-020MA (DSPE-PEG-MAL) obtained from NOF Europe, Belgium) in 0.1 M ammonium acetate for a day under nitrogen. The product was lyophilized three times to remove ammonium acetate.

Dodecanoyl alanine was prepared according to the literature method (Liu et al., 2014). Briefly, 100 ml NaOH (1 M) and 1.34 g (0.015 mol) L-alanine were added into a one-neck flask. After the system was cooled to 0 °C, 3.31 ml (0.014 mol) dodecanoyl chloride was added dropwise to the mixture and maintained for 5 h at 0 °C. Then 16 ml hydrochloric acid (12 M) was added to the reaction and the white precipitate was filtrated. Finally the product was washed three times with deionized water and dried at 45 °C for 24 h.

2.4. Preparation of targeted niosomes loaded with albumin

Non-ionic surfactants, Span 60 (sorbitane-monostearate) and Solulan C24 (cholesteryl-poly-24-oyxyethylene-ether, Chemron Co. USA) were dissolved with cholesterol in hot 1:2 mixtures of chloroform and ethanol in a round-bottom flask. N-dodecyl-β-D-glucopyranose (GP, 9% (*w*/w) of total lipid), dodecanoyl-alanine (A, 5% (w/w) of total lipids) or pegylated-GSH (GSH, 5% (w/w) of total lipids) were added to prepare targeted niosomes (N-GP, N-A, N-GSH) (Dufes et al., 2004; Gaillard et al., 2014). For dual-targeted NPs (N-A-GP, N-A-GSH, N-GP-GSH) the content of ligands was 4–4% (w/w) of the total lipids. The removal of organic solvents by vacuum pump yielded a thin lipid film layer. The dry lipid film was hydrated with phosphate buffer (PBS; KCl 2.7 mM, KH_2PO_4 1.5 mM, NaCl 136 mM, $Na_2HPO_4 \times 2\ H_2O$ 6.5 mM, pH 7.4) containing Evans blue-labeled bovine serum albumin (EBA, 67 kDa; 0.167 mg/ml EB, 10 mg/ml BSA). For transmission electron microscopy niosomes with the electron dense lanthanum nitrate (433 Da), as a cargo, were prepared. The mixture was heated at 40 °C in a water bath and sonicated for 25 min. The suspension was forced through a polycarbonate filter (Whatman filter, 13 mm, 100 nm pore size) by lipid extrusion technique (high pressure thermobarrel extruder, Lipex Biomembranes Inc. USA) to yield vesicles. The non entrapped cargo was removed by ultracentrifugation (123,249 *g*, 6 h, 4 °C), the pelleted niosomes were resuspended in PBS or DMEM medium and stored at 4 °C.

2.5. Preparation of targeted niosomes loaded with lanthanum and lanthanum measurement

For transmission electron microscopy experiments niosomes with the electron dense lanthanum nitrate hexahydrate (433 Da), as a cargo were prepared by hydrating the lipid film with PBS containing 5 mg/ml lanthanum. The lanthanum content of the particles was determined by a quadrupole Agilent 7700× inductively coupled plasma mass spectrometer (ICP-MS), was used for trace element analysis. The sample introduction system consisted of an Agilent I-AS auto sampler and a Micro Mist pneumatic nebulizer in a Peltier-cooled Scott-type spray chamber. The sample uptake rate was 400 µL/min. The ICP plasma and interface parameters were set up as follows: RF forward power: 1550 W, plasma gas flow rate: 15.0 L/min, carrier gas flow rate: 1.05 L/min, sampling depth: 10.0 mm. Ultra trace quality HNO_3 acid was also used for the acid dissolution of the samples at 180 °C. The digestion time was one hour. Signal tuning was performed by Agilent (No. G1820-60410) solutions, whereas calibration was done using solutions prepared from an Inorganic Ventures (Christiansburg, Virginia, USA) IV-ICPMS-71A multielement stock standard. The 99.996% purity argon gas used was purchased from Messer Hungarogáz (Hungary). Data processing was performed within the Agilent Mass Hunter (Santa Clara, California, USA) software.

2.6. Characterization of niosomes: Size, charge and encapsulation efficiency

The NPs were characterized for particle size and zeta potential using dynamic light scattering (Malvern Zetasizer Nano ZS, Worcestershire, UK). Before measurements the niosome samples were diluted in PBS to a final concentration of 200 µg/mL. The means of particle size and zeta potential data were calculated from the average of three measurements per sample. To determine the amount of encapsulated dye in the NPs, EBA was released from the niosomes with 50% v/v ethanol and measured by spectrofluorometer (Fluorolog 3, Horiba Jobin Yvon) at 584 nm excitation and 663 nm emission wavelengths. The concentrations were determined from a standard fluorescence calibration curve ($r^2 = 0.9985$). The encapsulation efficiency % (EE%) was calculated by the following equation:

$$EE\% = \frac{\text{Amount of EBA in the NP sample}}{\text{Amount of EBA in the hydrating buffer}} \times 100$$

2.7. Characterization of niosomes: Transmission electron microscopy

Aliquots of the niosome samples (10 µL) were placed on formvar carbon 400-mesh copper grids (Electron Microscopy Sciences, Washington, PA, USA). Images were taken on a JEOL JEM-1400 transmission electron microscope (JEOL Ltd., Japan) operating at 120 kV. Images were captured routinely at magnifications of 20,000×, 25,000× and 30,000×, and analyzed with a SightX Viewer Software (EM-15300SXV Image Edit Software, JEOL Ltd., Tokyo, Japan).

2.8. Characterization of niosomes: Atomic force microscopy

A two-beam interference lithography arrangement was applied to generate sub-micrometer periodic intensity modulation in the laser beam irradiating the samples (Csete et al., 2007). The fourth harmonic of a Nd:YAG laser (λ_{FH} = 266 nm, t = 10 ns, f = 10 Hz) was diffracted impinged on a reflective grating (PUV 1200, Spectrogon), and the first order diffracted beams were recombined at the sample surface. The samples were NBK7 substrates evaporated by gold-silver bimetallic layers, and spin-coated by polycarbonate.

The samples were silicone wafer substrates spin-coated by polycarbonate, which were treated by s-polarized beams, to produce linear gratings as described earlier (Csete et al., 2007). The laser treated surfaces were scanned by atomic force microscopy (AFM) operating in digital pulsed force mode (DPFM, Witec GmbH, Germany). The advantage of this scanning mode is the possibility to map the micromechanical properties of the surface with high resolution. We applied standard PFM tips (NSC 18/NoA1, 2.5 N/m) and collected pictures about the topography and adhesion, which revealed that the adhesion is stronger in the valleys of the linear grating, thus facilitating the deposition of particles.

To examine niosomes the samples with laser-grated surfaces were completely immersed in fresh PBS solutions containing niosomes. Incubation of the samples in the solutions lasted for 1 h at 37 °C, then all samples were washed three times in sterile distilled water on a horizontal shaker and finally allowed to dry overnight at room temperature. An AFM (XE-100, PSIA Corp.) operating in tapping-mode was applied to detect the attached biomolecules using tapping-mode NT-MDT tips (NSG11, 5.5 N/m, 150 kHz, NT-MDT).

2.9. RNA isolation and quality control

Rat brain microvessels were isolated as described in our previous article (Veszelka et al., 2007). Primary rat brain endothelial cells (RBEC; isolated according to the method described in section *2.11.* and in our previous studies (Veszelka et al., 2007; Nakagawa et al., 2009; Walter et al., 2015) were cultured for 5 days in 10 cm dishes. After reaching confluency the cells were scraped, collected and cell pellets were used for total RNA isolation using RNAqueous-4PCR Kit (Ambion, Life Technologies, Austin, TX, USA) with DNase1 (RNase-free) treatment according to the manufacturer's instructions. The concentrations

and purity of the DNase-treated RNA samples were assessed by a NanoDrop ND-1000 spectrophotometer (NanoDrop Technologies, Rockland, DE). The integrities of the isolated RNAs were characterized using Bioanalyzer 2100 (Agilent Technologies, Santa Clara, CA). The RNA integrity numbers (RIN) were between 9.2 and 10 in the case of all studied RNA samples.

2.10. Quantitative real-time polimerase chain reaction and data analysis

In all cases, cDNA synthesis was performed on 1 µg total RNA samples by High Capacity cDNA Reverse Transcription Kit (Life Technologies) using random hexanucleotide primers and MultiScribe Reverse Transcriptase in the presence of RNase inhibitor according to the manufacturer's protocols. The expression of the genes of transporters for alanine (sodium-coupled neutral amino acid transporters, *Snat1/Slc38a1*, *Snat2/Slc38a2*, *Snat5/Slc38a5*; neutral amino acid transporters, *Asct1/Slc1a4*, *Asct2/Slc1a5*) and the genes of transporters for glucose (*Glut1/Slc2a1*, *Glut3/Slc2a3*, *Glut5/Slc2a5*) were analyzed by quantitative PCR using TaqMan Low Density Array 384-well microfluidic cards preloaded with TaqMan Gene Expression Assays (Life Technologies). Quantitative real-time PCRs (qPCR) were performed by ABI TaqMan Universal Master Mix (Life Technologies) using the ABI Prism 7900 system (Applied Biosystems, Life Technologies). qPCR data were analyzed using the ABI SDS 2.0 software (Applied Biosystems, Life Technologies). In all samples the expression of genes was normalized to 18S rRNA, which was used as an endogenous control ($\Delta C_t = C_{tgene} - C_{t18S\ rRNA}$). Expression values of studied genes were determined based on the normalized expression of genes calculated with $2^{-\Delta Ct}$ formula which were correlated to the lowest normalized expression measured by the applied qPCR method. For quantification of relative expression level of genes of interest, the normalized expression data were analyzed using the comparative $\Delta\Delta C_t$ method (Livak and Schmittgen, 2001; Tóth et al., 2014).

2.11. Primary cell cultures and BBB model for permeability studies

Isolation of RBEC cells, glia and pericytes, and the construction of the *in vitro* BBB model were performed according to the method described in our previous studies (Nakagawa et al., 2009; Walter et al., 2015). After isolation cells were seeded on culture dishes (Corning, Costar, New York, NY, USA) coated with 100 µg/mL collagen type IV and 100 µg/mL fibronectin in sterile distilled water. RBEC cells were cultured in DMEM/HAM's F-12 (Gibco, Life Technologies, Carlsbad, CA, USA), 15% plasma-derived bovine serum (PDS, First Link, Wolverhampton, UK), 100 µg/mL heparin, medium supplement with 5 µg/mL insulin, 5 µg/mL transferrin, 5 ng/mL sodium selenite (ITS, Pan-Biotech Gmbh., Germany), 1 ng/mL basic fibroblast growth factor (bFGF, Roche, Basel, Switzerland) and 50 µg/mL gentamycin. During the first three days of culture the medium of RBEC cells contained 3 µg/mL puromycin to eliminate P-glycoprotein negative, contaminating cell types (Perrière et al., 2005).

For the permeability studies a triple co-culture BBB model was used (Nakagawa et al., 2009). For this model, in addition to brain endothelial cells, primary rat brain pericytes were isolated using the same method as for brain endothelial cells, except that pericytes were plated onto uncoated culture dishes and did not receive puromycin. Primary cultures of rat glial cells were prepared from one-day-old Wistar rats and passaged (8.5×10^4 cells/cm^2) to 12 well plates (Corning, Costar, New York, NY, USA) coated with collagen type IV (100 µg/ml in sterile distilled water). Rat glial cells were cultured for two weeks before using them for the co-culture model (Veszelka et al., 2007). Pericytes and glial cells were cultured in DMEM/HAM's F-12 supplemented with 10% fetal bovine serum (FBS, Pan-Biotech GmbH) and 50 µg/mL gentamycin. To prepare the co-culture model, pericytes at P2 were passaged (1.5×10^4 cells/cm^2) to the collagen coated bottom side of tissue culture inserts (Transwell, polycarbonate membrane, 3 µm pore size,

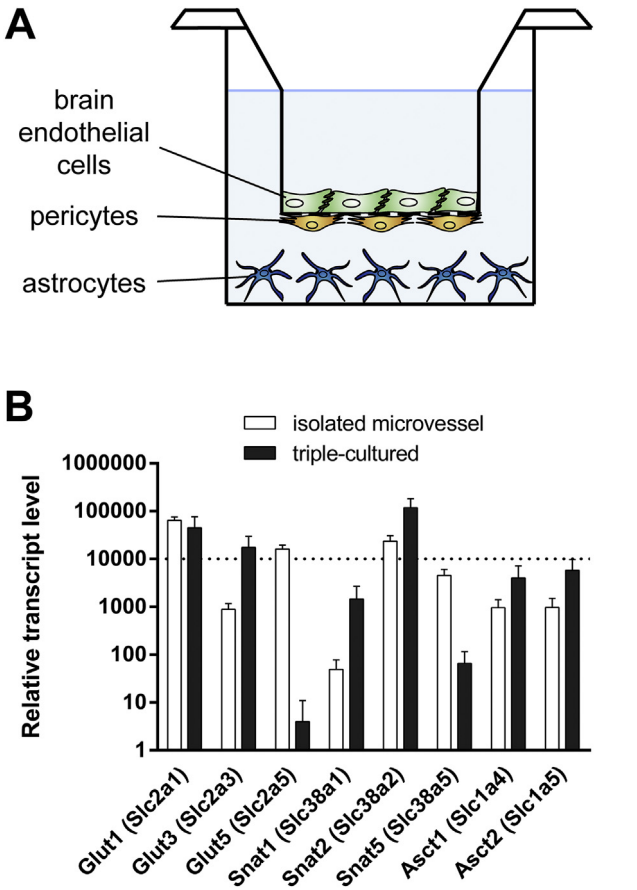

Fig. 1. (A) Schematic drawing of the BBB co-culture model. (B) Expression of genes encoding solute carriers for glucose and alanine in isolated rat brain microvessels and in primary rat brain endothelial cells in co-culture with rat pericytes and astrocytes.

Corning Costar) and brain endothelial cells were seeded (7.5×10^4 cells/cm^2) to the upper side of the Matrigel (growth factors reduced, Corning Costar, USA) coated membranes. Then the inserts containing brain endothelial cells and pericytes on the two sides of the membrane were placed to 12 well plates in which glial cells were grown at the bottom (Fig. 1A). Both the upper and lower fluid compartments of this system received endothelial culture medium supplemented with 550 nM hydrocortisone and the three types of cells were cultured together for four days before permeability experiments (Nakagawa et al., 2009; Walter et al., 2015).

2.12. Cell viability assay

Kinetics of RBEC cell reaction to niosome treatment were monitored by impedance measurement (RTCA-SP instrument; ACEA Biosciences, San Diego, CA). Impedance measurement is label-free, real time, non-invasive, and correlates linearly with adherence and growth of cells. After background measurements, cells were seeded at a density of 6×10^3 cells/well in collagen coated 96-well plates with integrated gold electrodes (*E*-plate 96, ACEA Biosciences). Cells were cultured for 5–7 days in CO_2 incubator at 37 °C and monitored for 4 h. Triton X-100 detergent (10 mg/mL) was used as a reference compound inducing cell toxicity. Cell index was defined as $R_n - R_b$ at each time point of measurement, where R_n is the cell-electrode impedance of the well when it contains cells and R_b is the background impedance of the well with the medium alone. Cell index values reflect cell number and viability (Kiss et al., 2013; Bocsik et al., 2016).

2.13. Measurement of the uptake of niosomes in RBEC cells

The RBEC cells were cultured in 24 well plates (Corning Costar, USA) at the density of 3×10^4 cells/well. The confluent monlayers were incubated with 10 mg/mL niosome solutions (N, N-GP, N-A, N-GSH, N-A-GP, N-GP-GSH, N-A-GSH) in culture medium for 4 h. The uptake of single or dual-targeted niosomes in RBEC cells was tested at 4 °C and 37 °C. To elucidate the uptake mechanisms of targeted niosomes cells were co-treated with metabolic inhibitor sodium azide (1 mg/ml) or pretreated with endocytosis inhibitors, filipin (15 min, 6 μM) and cytochalasin D (1 h, 20 μM) in culture medium. To study the role of the surface charge in cellular uptake of NPs we digested the surface glycocalyx of RBECs with neuraminidase (1 U/ml, 1-hour pretreatment), or treated the cells with 54 μM cationic lipid 1-(4-trimethylammoniumphenyl)-6-phenyl-1,3,5-hexatriene (TMA-DPH; Molecular Probes, Life Technologies) for 30 min before the uptake. After incubation with niosomes RBECs were washed three times with ice cold PBS supplemented with 1% BSA and once with acid stripping buffer (glycine 50 mM, NaCl 100 mM, pH 3) to remove cell surface associated niosomes. Finally cells were lysed in PBS with Triton X-100 detergent (10 mg/mL) and the fluorescent signal was detected with a spectrofluorometer (Horiba Jobin Yvon Fluorolog 3, Edison New Jersey, USA) at 584 nm excitation and 663 nm emission wavelengths.

2.14. Visualization of the uptake of niosomes in RBEC cells

To visualize the cellular uptake of the fluorescent particles RBECs were grown on glass bottom Petri dishes coated with Matrigel and treated with 10 mg/mL niosomes for 4 h. The stain cell nuclei H33342 dye (1 μg/mL; 10 min) was used. After incubation living cells were washed three times with Ringer-Hepes buffer (118 mM NaCl, 4.8 mM KCl, 2.5 mM $CaCl_2$, 1.2 mM $MgSO_4$, 5.5 mM D-glucose, 20 mM Hepes, pH 7.4) supplemented with 1% PDS and examined with a confocal laser scanning microscope (Olympus Fluoview FV1000, Olympus Life Science Europa GmbH, Hamburg, Germany).

The cellular uptake of targeted NPs was also examined by transmission electron microscopy. RBECs were grown on culture inserts and treated untargeted (N) or dual-targeted (N-A-GSH) niosomes (10 mg/ml) with lanthanum cargo for 4 h at 37 °C. Control cells were treated 0.2 μg/mL lanthanum, the same concentration entrapped in the niosomes. After incubation, RBECs were briefly rinsed in 0.1 M phosphate buffer (PB), then fixed in 4% paraformaldehyde + 2.5% glutaraldehyde dissolved in 0.1 M PB at 4 °C for 30 min. After rinsing in 0.1 M PB the inserts were removed from the tissue culture plates and transferred into 50 ml centrifuge tubes containing 0.1 M PB and kept at 4 °C overnight. Cells on the membranes were postfixed in 1% aqueous OsO_4 for 1 h at room temperature, washed in tri-distilled water for 10 min and processed in a graded series of ethanol (50%, 70%, 90%, 96%, 100%, 100%) for 10 min in each solution. Then, 4–5 mm small pieces of the membranes with cells were embedded in Durcupan. Semithin (0.5 μm) sections were cut from the blocks on a Reichert OM-U2 ultramicrotome, which were stained to localize the cell layers on the membranes. Next, ultrathin section (60 nm) were cut on a Leica Ultracut S ultramicrotome, mounted either on formvar coated single slot or uncoated 300 mesh copper grids, and stained with 2% uranyl acetate for 15 min. Sections were examined in a JEOL JEM 1400 Plus electron microscope operated at 100 kV accelerating voltage. Digital images were taken with a Matataki 8 MPix CCD camera at 16-bit gray scale color depth and saved in uncompressed TIFF format.

2.15. Permeabilty of niosomes across the BBB co-culture model

The tightness of the BBB co-culture model was verified by measurement of transendothelial electric resistance (TEER) by EVOM voltohmmeter (World Precision Instruments, Sarasota, 45 FL, USA) combined with STX-2 electrodes. When high TEER values ($539 \pm 71\ \Omega \times cm^2$) were obtained, the model was used for experiments. Cells were treated in the upper, donor compartment (0.5 mL) with single or dual-targeted niosomes (10 mg/mL) diluted in phenol red free DMEM F12 supplemented with 1% PDS and 1% ITS for 4 h. After incubation samples were collected from the lower, acceptor compartments (1.5 mL) and measured with spectrofluorometer (Horiba Jobin Yvon Fluorolog 3) at 584 nm excitation and 663 nm emission wavelengths. The apparent permeability coefficients (P_{app}) were calculated as described previously (Bocsik et al., 2016) by the following equation:

$$P_{app}(\mathrm{cm/s}) = \frac{\Delta[C]_A \times V_A}{A \times [C]_D \times \Delta t}$$

Briefly, P_{app} (cm/s) was calculated from the concentration difference of the NPs in the acceptor compartment ($\Delta[C]_A$) after 4 h. $[C]_D$ is the concentration in the donor compartments at 0 h, V_A is the volume of the acceptor compartment (1.5 mL), and A is the surface area available for permeability (1.1 cm^2).

2.16. Measurement of plasma membrane fluidity

RBECs grown in culture dishes were treated with N and N-A-GSH (10 mg/ml) diluted in culture medium for 4 h at 37 °C in a CO_2 incubator. The cells were washed twice with PBS, collected by trypsinization, and resuspended in Ringer-Hepes buffer. The density of cells was set by absorbance measurement to $OD_{360} = 0.1$ (Hewlett Packard 8452A Diode Array Spectrophotometer). Cells were labeled with 0.2 μM TMA-DPH for 5 min. Fluorescence anisotropy was measured on a T-format fluorescence spectrometer (Quanta Master QM-1, Photon Technology International, Princeton, NJ, USA). Excitation and emission wavelengths were 360 and 430 nm, respectively (5 nm and 6 nm slits). Cells were kept at 37 °C under stirring conditions. Anisotropy data were acquired in every second for 5 min, then benzyl alcohol (50 mM; Merck, Darmstadt, Germany), a strong membrane fluidizer, was added and data were acquired for another 5 min. The average of 50 anisotropy measurements in the last 1 min of each treatments was calculated and compared (Kiss et al., 2014; Lénárt et al., 2015).

2.17. In vivo imaging of targeted niosomes

Ten-week old male CD1-Foxn1nu nude mice (Winkelmann, Borchen, Germany) were used for *in vivo* imaging. Animals were kept under conventional controlled conditions (22 °C, 55% humidity, day-night rhythm) and had free access to a standard diet (ssniff Spezialdiäten GmbH, Soest, Germany) and tap water. A time domain *in vivo* small animal fluorescence imager Optix™ (ART, Montreal, Canada; Keren et al., 2008; Kumar et al., 2008) was used to monitor the brain penetration of the EBA cargo of niosomes in real-time and over several time points in the same animal. Animals were placed in prone position on the table of the imager. Anesthesia was maintained during the fluorescence detection by offering an oxygen-isoflurane gas mix *via* a small mask. EBA encapsulated in different niosomes (N, N-A, N-GP, N-A-GP) were injected intravenously (100 μL, tail vein). Fluorescence measurement to visualize the EBA was performed repeatedly after niosome injection at defined time points up to 24 h (0, 10 and 30 min, 3, 6 and 24 h). The animals were returned to their cage and provided access to food and water between the longer measurement points. Head-detector distance was equal in all measurements. The red fluorescent signal of EBA was detected over the whole body of living anesthetized mice in 0.5 mm steps. For fluorescence detection, a time-correlated single-photon counting system (TCSPC-130) was used. Intensity units were normalized for the same excitation power and excitation time per raster point (integration time).

2.18. Statistical analysis

Data are presented as means ± SEM or SD. Values were compared

using one-way or two-way analyses of variances following Dunnett or Bonferroni multiple comparison posttests (GraphPadPrism 5.0; GraphPad Software, USA). Changes were considered statistically significant at $P < 0.05$. All experiments were repeated at least two times and the number of parallel samples was 4–10.

3. Results

3.1. Expression of selected Slc genes coding nutrient transporters

We verified the expression of genes for Slc transporters carrying glucose and alanine in the BBB co-culture model and in freshly isolated rat brain microvessels (Fig. 1B). Among the carriers of glucose the expression level of the gene *Glut1*, coding the predominant glucose transporter at the BBB, was the highest, followed by *Glut5* and *Glut3* in brain microvessels. In RBECs the relative transcript levels for *Glut1* and *Glut3* were also high, while that of *Glut5* was very low. All the tested neutral amino acid transporter genes were detectable in both brain microvessels and RBECs. The mRNA of *Snat2* was expressed at the highest level in both models. From the tested eight genes only in two cases, for *Glut5* and *Snat5,* were transcript levels much lower in RBECs than in brain microvessels **(**Fig.1B**).**

3.2. Characterization of niosomes

Table 1 summarizes the main physicochemical properties of the untargeted (N), single ligand targeted (N-GP, N-A, N-GSH), and dual-ligand targeted (N-A-GSH, N-A-GP, N-GP-GSH) niosomes (for schematic drawing see Fig. 2). The average diameter of the niosomes varied between 92 and 107 nm. All groups had low polydispersity index, indicating a relatively narrow size distribution. The zeta potentials of niosomes were between −3 and −4 mV, except those decorated with GSH ligand (N-GSH, N-A-GSH, N-GP-GSH), which had a more negative surface charge, around −7 mV. The encapsulation efficiency of the cargo EBA was in the range of 4.6–10.4%. The amount of the encapsulated large hydrophilic biomolecule EBA was between 0.5 and 1.1 mg/100 mg nanoparticle total weight (Table 1). The morphology of the NPs was spherical as observed by transmission electron microscopy (Fig. 3A) and atomic force microscopy (Fig. 3B). No aggregation was visible.

The stability of untargeted niosome loaded with EBA was followed for six months. The size of niosomes changed from 92.8 ± 1.8 nm to 119.5 ± 1.9 nm during this period. At 6 months the polydispersity index was 0.30 ± 0.003 indicating monodispersity, and the zeta potential (−4.03 ± 0.49 mV *vs.* −3.67 ± 0.09 mV) and the encapsulation efficiency (11.5% *vs.* 9.21%) have changed minimally. Based on these data the niosome preparation can be considered as stable regarding size, encapsulated cargo and aggregation for at least 6 months.

3.3. Effect of niosomes on cell viability of RBECs

Incubation of RBECs with non-targeted or targeted niosomes in the 0.3–10 mg/mL concentration range for 4 h did not decrease the impedance of cell layers reflecting good cell viability (Fig. 4). For further experiments we selected the 10 mg/mL concentration, which can be considered as a safe concentration for all niosome groups.

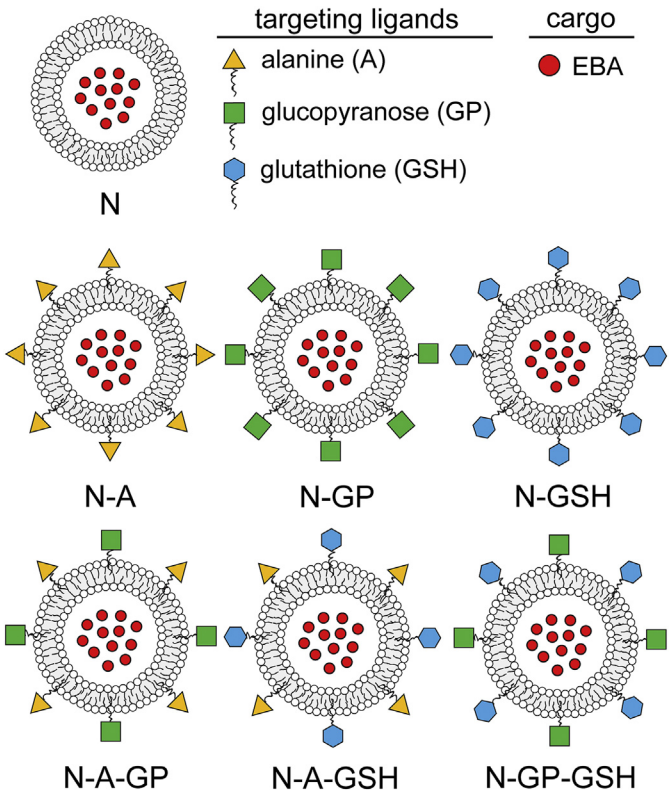

Fig. 2. Schematic drawing of non-targeted (N), single ligand targeted (N-A: alanine-, N-GP: glucopyranose-, N-GSH: glutathione-targeted) and dual-targeted niosomes (N-A-GP: glucose-alanine-, N-A-GSH: alanine-glutathione-, N-GP-GSH: glucose-glutathione-targeted).

3.4. Uptake of the cargo of single and dual-targeted niosomes in RBEC

The uptake of the large hydrophilic free EBA was very low in brain endothelial cells, only 1.5% of the EBA uptake in cells treated with non-targeted niosome containing the cargo (N) (Fig. 5). As compared to non-targeted niosomes, the uptake of EBA in RBECs treated with nanovesicles decorated with alanine, glucopyranose or glutathione was higher (N-A: 131%, N-GP: 130%, N-GSH: 191%). The presence of dual-ligands statistically significantly increased the cellular concentration of EBA in brain endothelial cells in the case of N-A-GP (293%) and N-A-GSH groups (249%), but not in the N-GP-GSH group.

Table 1
Characterization of the non-targeted and targeted niosomes.

Niosomes	Size (nm)	Polydispersity index	Zeta potential (mV)	Encapsulation efficiency (%)	Encapsulated BSA (mg/100 mg NP)
N	106 ± 10	0.18 ± 0.04	−3.41 ± 0.50	8.47 ± 3.24	0.85 ± 0.33
N-A	92 ± 40	0.18 ± 0.01	−4.36 ± 0.60	7.54 ± 3.57	0.75 ± 0.36
N-GP	98 ± 14	0.20 ± 0.04	−4.19 ± 0.29	4.90 ± 0.52	0.49 ± 0.05
N-GSH	107 ± 11	0.17 ± 0.02	−7.39 ± 0.77	10.43 ± 6.17	1.04 ± 0.62
N-A-GSH	103 ± 50	0.18 ± 0.01	−7.14 ± 1.15	6.14 ± 2.60	0.61 ± 0.26
N-A-GP	94 ± 10	0.17 ± 0.01	−3.83 ± 1.03	10.87 ± 0.53	1.09 ± 0.05
N-GP-GSH	101 ± 80	0.17 ± 0.01	−6.40 ± 1.27	4.66 ± 2.53	0.47 ± 0.25

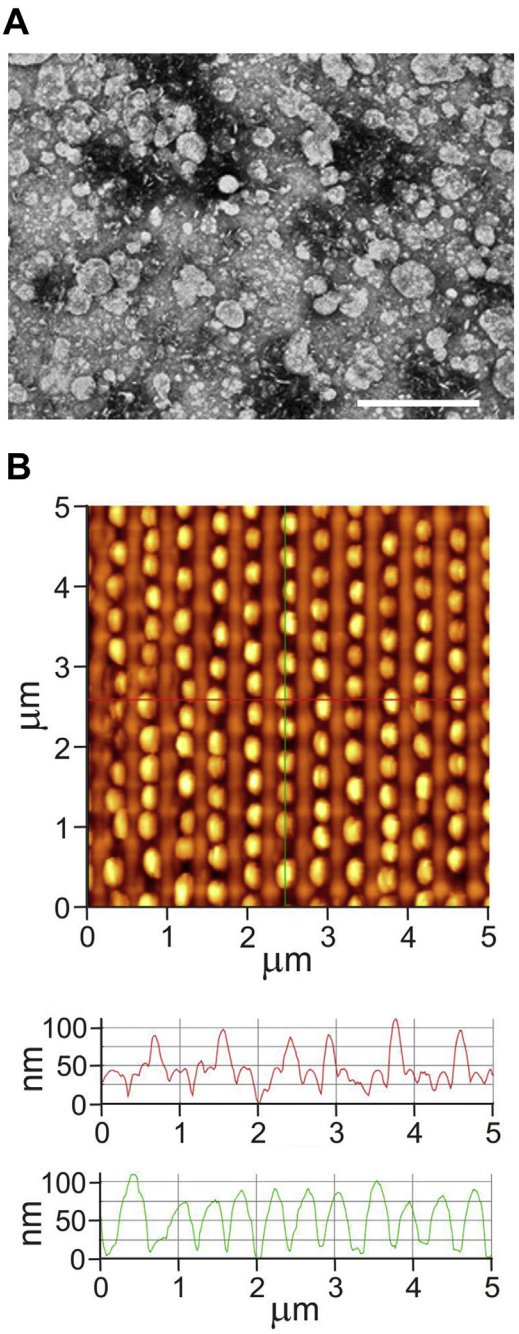

Fig. 3. (A) Transmission electron microscopy image of niosomes, bar: 500 nm. (B) Atomic force microscopy image of niosomes.

3.5. Penetration of the cargo by targeted niosomes across a BBB co-culture model

The permeability of the BBB model for EBA was also very low (0.13×10^{-6} cm/s) reflecting a tight barrier (Fig. 6). This P_{app} value for EBA, a transendothelial marker molecule, is in accordance with our previous results (Walter et al., 2015). The encapsulation of EBA in non-targeted niosomes (N) increased the permeability of the cargo through brain endothelial cells (0.28×10^{-6} cm/s). Labeling the particles with single ligands resulted in further increase in the penetration of EBA across the BBB model (N-A: 1.18×10^{-6} cm/s; N-GP: 1.01×10^{-6} cm/s; N-GSH: 1.29×10^{-6} cm/s). The amount of EBA cargo that crossed brain endothelial cells was increased 17-fold in case of the N-A-GSH group (2.26×10^{-6} cm/s) and 14-fold in the N-A-GP group (1.83×10^{-6} cm/s) as compared to the EBA group (Fig. 6). The combination of GP-GSH ligands was not efficient to elevate EBA penetration across the BBB model. Based on the results, the N-A, N-GSH and N-A-GSH groups were selected for further *in vitro* experiments.

3.6. Cellular uptake: Visualization

Since EBA, our model cargo gives a red fluorescent signal (Uyama et al., 1988), the uptake of free EBA and EBA encapsulated in nanovesicles (N, N-A-GSH) was visualized in RBECs by confocal microscopy (Fig. 7A). Red fluorescence was detected in cells treated with dual-targeted N-A-GSH niosomes indicating uptake of the cargo. Less fluorescent signal was seen in the non-targeted vesicle (N) group, while the cellular entry of free dye (EBA) was barely detectable.

For transmission electron microscopy the cells were treated with free lanthanum (LA), lanthanum entrapped non-targeted niosomes (N) and vesicles labeled with dual-ligands containing lanthanum (N-A-GSH) (Fig. 7B). The particles were non toxic (data not shown) and their physicochemical properties (N: 110 nm, −2.25 mV; N-A-GSH: 115 nm, −5.08 mV) were similar to the niosomes filled with EBA. The concentration of lanthanum was equal in each groups. More dark precipitates and structures can be seen in cells treated with N-A-GSH compared to the untargeted nanoparticle (N) and lanthanum groups.

3.7. Cellular uptake: Temperature dependence and metabolic inhibition

To test the temperature dependence of the cellular uptake of nanovesicle encapsulated EBA, cells were treated with selected niosomes (N, N-A, N-GSH, N-A-GSH) at both 4 °C and 37 °C (Fig. 8). At 37 °C the EBA uptake was significantly higher in all targeted nanovesicle groups (N-A: 119%, N-GSH: 150%, N-A-GSH: 308%) compared to the non-targeted group (N: 100%). Decreased EBA uptake was seen in RBECs at 4 °C (N-A: 36%, N-GSH: 55%, N-A-GSH: 17%) as compared to the non-targeted group at 37 °C. Treatment of the cells with metabolic inhibitor sodium azide resulted in lower uptake of the cargo (N-A: 88%, N-GSH: 113%, N-A-GSH: 81%) compared to data measured at 37 °C in the same treatment groups (Fig. 8).

3.8. Cellular uptake: Inhibition of endocytosis

Two inhibitors of endocytosis (Ivanov, 2008) were used to further elucidate the mechanism of cellular uptake of EBA after treating the cells with dual-targeted N-A-GSH particles (Fig. 9A). Filipin, which inhibits lipid raft/caveolae-mediated endocytosis, slightly, but statistically significantly decreased the uptake of cargo in RBECs (94% of the control group). Cytochalasin-D, a common inhibitor of endocytosis by blocking F-actin depolymerization, also induced a partial, but significant inhibition of EBA uptake (80% as compared to the control group).

3.9. Cellular uptake: Modification of cell surface charge

We modified the surface charge of cultured brain endothelial cells by digestion of the surface glycocalyx with neuraminidase enzime (Singh et al., 2007) and treatment with a cationic lipid, TMA-DPH (Ribeiro et al., 2012). Surface charge alterations in RBECs did not affect the cellular uptake of EBA after treatment with non-targeted NPs as compared to the control, untreated group (Fig. 9B). In contrast, both modifications increased significantly the uptake of EBA in brain endothelial cells after incubation with N-A-GSH niosomes (Fig. 9B). The uptake of EBA was increased by 16%, after treatment of RBECs with neuraminidase and by 19% after incubation with TMA-DPH, as compared to untreated cells in the N-A-GSH nanoparticle group.

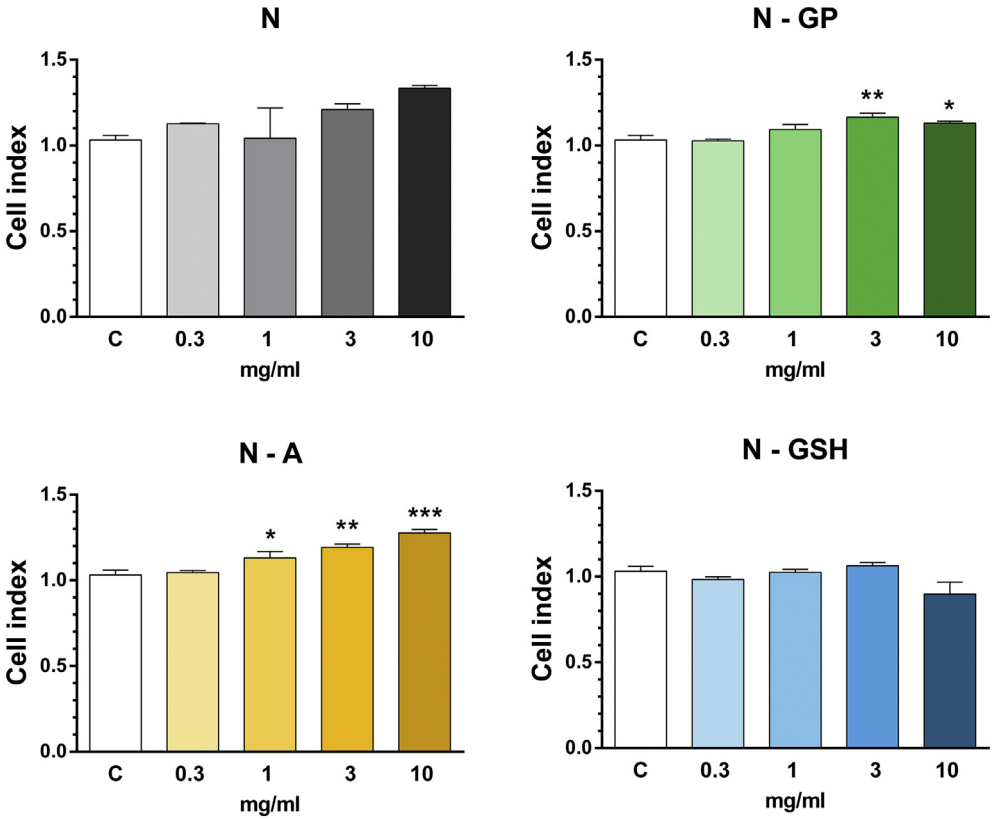

Fig. 4. The effect of non-targeted (N), alanine-targeted (N-A), glucopyranose-targeted (N-GP) and glutathione-targeted (N-GSH) niosomes on the viability of brain endothelial cells after 4-hour incubation. Values presented are means ± SEM. Statistical analysis: ANOVA followed by Dunnett's posttest, $^{*}P < 0.05$, $^{**}P < 0.01$, $^{***}P < 0.001$, compared to control group, $n = 8$. C: medium treated control group.

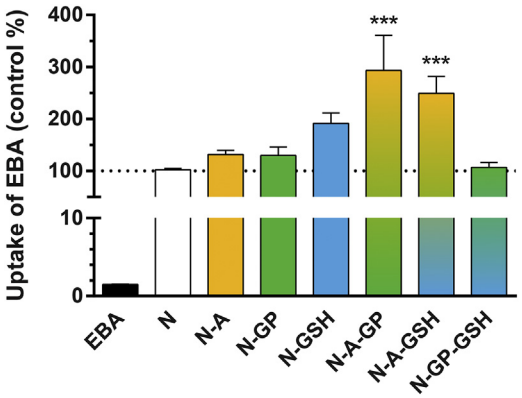

Fig. 5. The uptake of non-targeted (N), single- (N-A, N-GP, N-GSH) and dual-targeted (N-A-GP, N-A-GSH, N-GP-GSH) niosomes in brain endothelial cells after 4-hour incubation. Values presented are means ± SEM. Statistical analysis: ANOVA followed by Dunnett's posttest, where $^{***}P < 0.001$, compared to non-targeted N group; $n = 10$.

3.10. Interaction of nanovesicles with RBECs: Plasma membrane fluidity

The membrane fluidity of brain endothelial cells, determined by fluorescence anisotropy (Kiss et al., 2014), was significantly decreased after 4 h treatment with N and N-A-GSH nanovesicles (Fig. 10) indicating increased cell membrane fluidity and a fusion process. The membrane fluidizer benzyl alcohol (30 mM) quickly and greatly reduced the TMA-DPH fluorescence anisotropy after 3 min compared to the control and niosome treated groups indicating maximal plasma membrane fluidity.

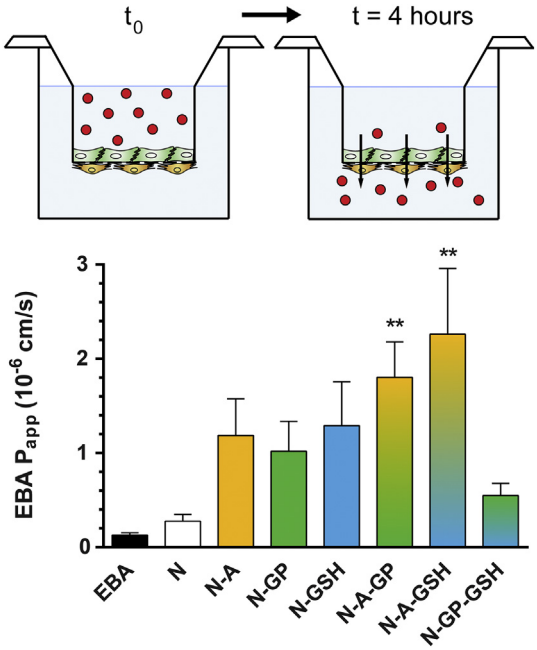

Fig. 6. Permeability of albumin cargo across the culture BBB model after treatment with different niosomes (10 mg/mL, 4 h). Values presented are means ± SEM. Statistical analysis: ANOVA, Dunnett's posttest. $^{**}P < 0.01$, compared to non-targeted N group; n = 10.

3.11. Imaging of EBA in mice after intravenous injection of targeted niosomes

Brain penetration of the red fluorescent EBA was measured by imaging in nude mice. Free EBA and EBA encapsulated in targeted and non-targeted niosomes were injected intravenously. There was no

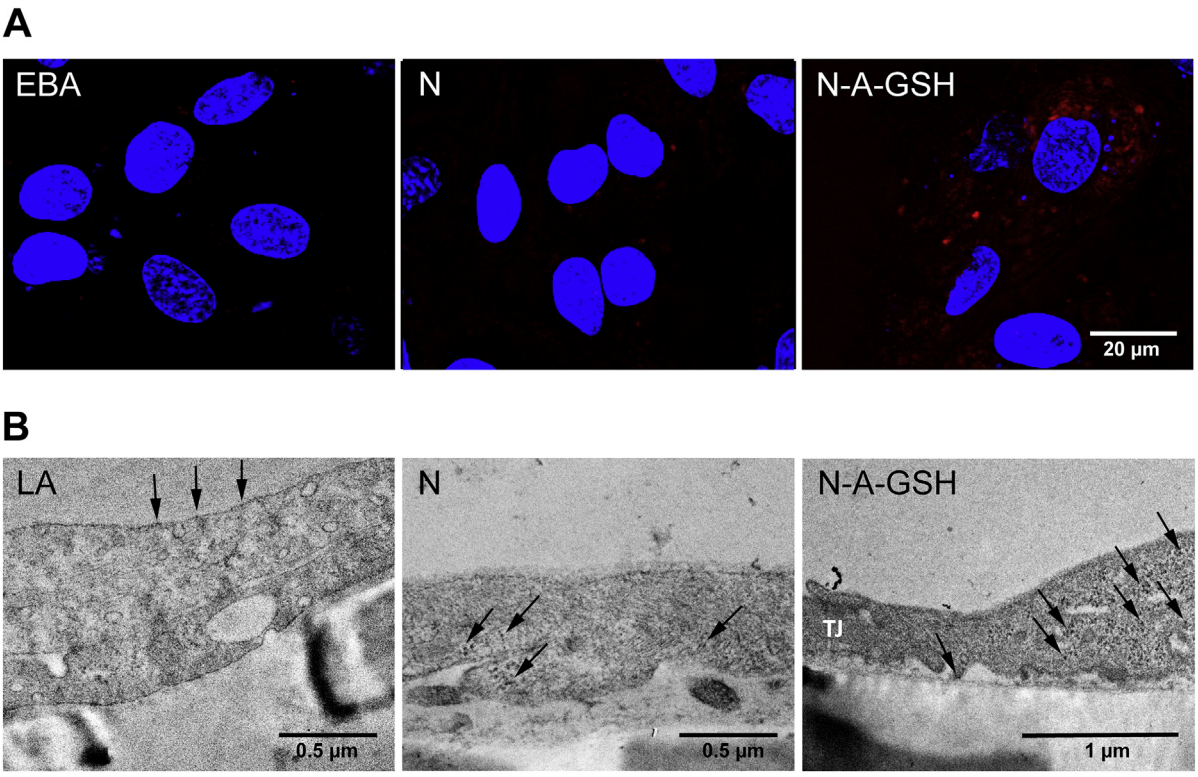

Fig. 7. (A) Confocal microscopy images of cultured brain endothelial cells incubated with unencapsulated cargo (EBA, showing red fluorescence), non-targeted (N) or alanine-glutathione-targeted (N-A-GSH) niosomes for 4 h at 37 °C. Cell nuclei were stained with bis-benzimide (blue). Bar: 20 µm. (B) Transmission electron microscopy images of the uptake of free lanthanum (LA) and lanthanum (black arrows) encapsulated in non-targeted (N) or alanine-glutathione-targeted (N-A-GSH) niosomes in brain endothelial cells after 4 h incubation. Bar: 0.5 and 1 µm. TJ: tight junction. (For interpretation of the references to color in this figure legend, the reader is referred to the web version of this article.)

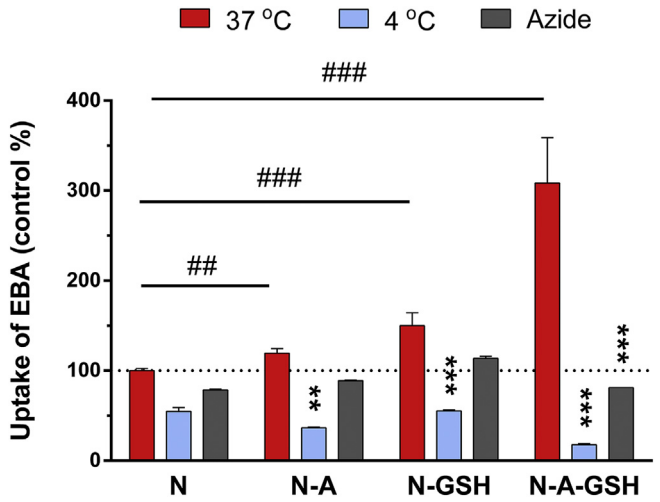

Fig. 8. The effect of temperature and metabolic inhibitor sodium azide (0.1%) on the uptake of EBA cargo in brain endothelial cells after 4 h incubation with non-targeted (N), alanine-targeted (N-A), glutathione-targeted (N-GSH) and alanine-glutathione-targeted (N-A-GSH) niosomes. Values presented are means ± SEM. Statistical analysis: two-way ANOVA, Bonferroni posttest. $^{*}P < 0.5$; $^{**}P < 0.01$; $^{***}P < 0.001$, compared to first column of each groups, $^{\#\#\#}P < 0.001$, compared to N treated group; $n = 4–6$.

significant accumulation of fluorescent signal in the brain area in the case of free EBA (Fig. 11). Encapsulation of EBA in non-targeted niosomes resulted in enhanced brain fluorescent intensity. The fluorescent signal in the brain area was further increased in the single ligand targeted N-A and N-GP groups. Fluorescent signal from EBA cargo in the dual-ligand targeted N-A-GP group was the highest as compared to all groups at all time points (Fig. 11). The differences between targeted, dual-ligand targeted and non-targeted niosomes were still visible at 24 h.

4. Discussion

4.1. Functionalization of NPs for BBB targeting by SLC ligands

Nanocarriers are intensively investigated as novel therapeutic tools to prevent or to treat CNS disorders (Masserini, 2013; Loureiro et al., 2015; Saraiva et al., 2016). The key problem for the effective targeting of NPs to brain is the proper functionalization of these carriers to cross the BBB (Wohlfart et al., 2012; Masserini, 2013; Kreuter, 2014). NPs accumulate in several organs, including liver, spleen, and kidney, and only specific BBB targeting can increase the ratio of nanocarriers penetrating the CNS (Saraiva et al., 2016). To ensure this relative brain specificity it is important to functionalize the NPs with targeting molecules which are substrates of physiological transporters of the BBB and able to trigger active and specific transport mechanisms to cross the BBB.

As compared to BBB receptors, SCLs are underresearched as molecular targets of CNS drug delivery systems (Rask-Andersen et al., 2013). The glucose consumption of the brain is the highest among the organs, and hexose transporters, especially GLUT-1 (SLC2A1), are highly expressed at the BBB (Campos-Bedolla et al., 2014). We confirmed that several glucose transporters were expressed in isolated rat brain microvessels and in brain endothelial cells of the BBB co-culture model with the *Glut1* gene showing the highest mRNA expression. N-dodecyl-β-D-glucopyranose was selected as a non-degraded glucose analog to decorate the niosomes. Using culture models of the BBB we found about 30% increase in the uptake and three-fold elevation in the permeability of the EBA cargo with N-GP, as compared to non-targeted niosomes, but

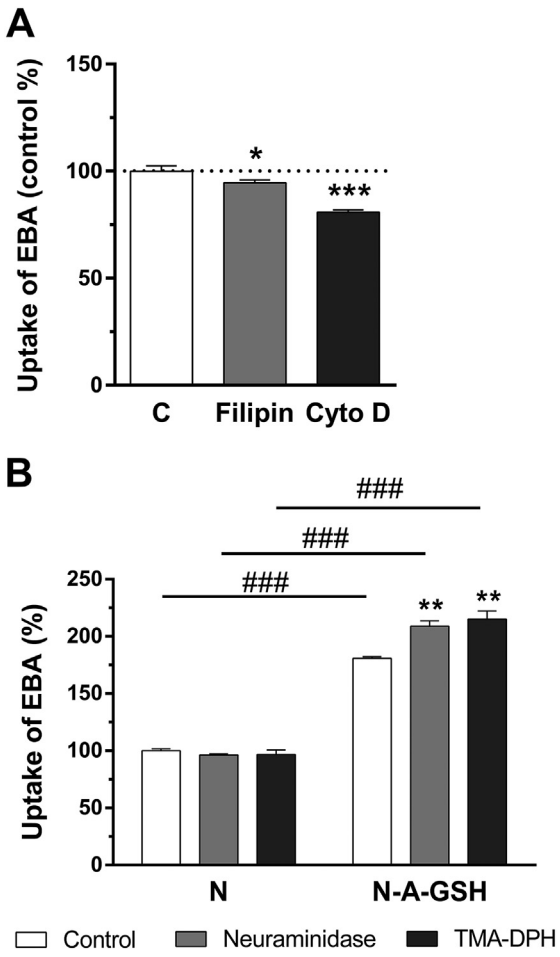

Fig. 9. (A) Inhibition of the uptake of EBA cargo with filipin (6 μM) or cytochalasin D (20 μM) in rat brain endothelial cells after 4 hours incubation with alanine-glutathione duale-targeted niosomes (N-A-GSH). Values presented are means ± SEM. Statistical analysis: ANOVA followed by Dunnett's posttest where $^{*}P < 0.5$; $^{***}P < 0.001$, compared to the control group; $n = 6$. (B) The effect of neuraminidase (1 U/ml) and TMA-DPH (30 mM) on the uptake of EBA cargo in brain endothelial cells incubated with non-targeted (N) and alanine-glutathione dual-targeted niosomes (N-A-GSH). Statistical analysis: two-way ANOVA, Bonferroni posttest. $^{**}P < 0.01$ compared to first column of each groups; $^{###}P < 0.001$, compared to N treated groups; $n = 6$.

these changes were statistically not significant. In mice the brain fluorescence of EBA significantly increased at 10 min and several fold elevation was observed until 24 h after tail vein injection of N-GP. Our *in vivo* results are in agreement with the findings of Dufes et al., who described that niosomes targeted with N-palmitoylglucosamine ligand enhanced the brain entry of the cargo vasoctive intestinal peptide in mice (Dufes et al., 2004). Small gold NPs covalently coated with β2-mercaptoethoxy-glucose entered and crossed cultured human brain endothelial cells better than non-brain endothelial cells (Gromnicova et al., 2013). Nanoparticles, including liposomes, micelles and solid polymeric NPs derivatized with different glucose analogs improve the delivery of encapsulated drugs or fluorescent dyes to the brain by targeting GLUTs as reviewed by Patching (2017) indicating the potential applicability of these SLCs.

The small neutral amino acid alanine, which is transported by several SLCs at the BBB (Campos-Bedolla et al., 2014), was selected as the other targeting ligand of the tested niosomes. The mRNAs of both the sodium coupled and neutral amino acid carriers were highly represented in brain microvessels and the BBB culture model. To our best knowledge, this is the first report indicating that NPs decorated with alanine as a targeting ligand elevated the uptake of the cargo in

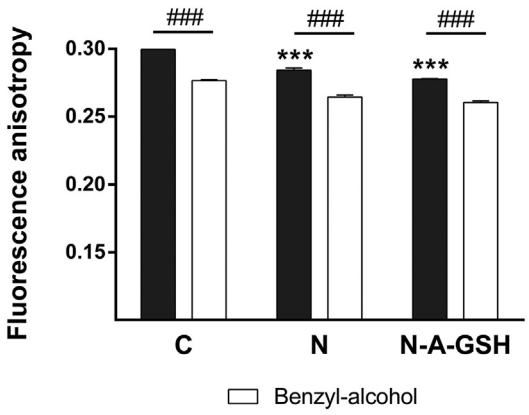

Fig. 10. The effect of non-targeted (N) and alanine-glutathione dual-targeted niosomes (N-A-GSH) and benzyl alcohol (30 mM) on plasma membrane fluidity measured by fluorescence anisotropy on living brain endothelial cell suspensions. Values presented are means ± SEM. Statistical analysis: two-way ANOVA, Bonferroni posttest. $^{***}P < 0.001$, all groups were compared to non-treated control (C); $^{###}P < 0.001$, compared to first column of each groups, $n = 3$.

cultured brain endothelial cells (Fig. 8) and its brain entry in mice (Fig. 11).

As a reference targeting ligand niosomes were also functionalized with glutathione. Labeling of niosomes with GSH-PEG significantly increased the uptake of EBA in primary RBECs (Fig. 8) and elevated four-fold the EBA permeability across the BBB culture model as compared to untargeted NPs (Fig. 6). These findings are supported by data showing that GSH targeting of liposomes elevated the uptake of carboxifluorescein in RBE4 rat brain endothelial cell line (Rip et al., 2014) and that of doxorubicin in hCMEC/D3 human brain endothelial cell line (Gaillard et al., 2014). GSH labeling also elevated the permeability of solid NPs across BBB culture models (Grover et al., 2014; Veszelka et al., 2017). The GSH-PEGylated liposomal drug delivery system was effective in rodent models for brain delivery of different drug cargos, like doxorubicin (Gaillard et al., 2014) or ribavirin (Maussang et al., 2016), indicating the *in vivo* applicability of GSH and the predictive value of *in vitro* BBB models.

4.2. Dual targeting of BBB transporters

In concordance with our hypothesis, dual labeling of niosomes with ligands of BBB transporters (N-A-GP and N-A-GSH) elevated the cargo uptake in RBECs and penetration across the BBB model as compared to both single ligand targeted or untargeted NPs. The effect of dual labeling of NPs with SLC substrates (N-A-GP) on brain uptake of cargo was the highest in the mouse study (Fig. 11). The cargo selected for our study, the large biomolecule albumin, has a negligible transport across the BBB in physiological conditions (Abbott et al., 2010). This is also reflected in the very low P_{app} value (0.1×10^{-6} cm/s) of the free EBA across the BBB model (Fig. 6), in accordance with our previous data (Deli et al., 2005; Walter et al., 2015; Veszelka et al., 2018). Free EBA cargo penetration to brain was also limited in mice (Fig. 11), as we demonstrated it in our previous study (Veszelka et al., 2003). It should be noted, that compared to small molecule permeability, the P_{app} value of EBA increased by dual targeted nanovesicles is still low (Fig. 11). We should consider however, that this limited EBA transport represent 10- and 20-fold increases in the P_{app} value or in the brain fluorescence intensity, respectively, of this low penetrant cargo.

As a possible mechanism, the combination of two different SLC transporter ligands on the niosomal surface may produce stronger vesicular docking to brain endothelial cells facilitating NP fusion and/or endocytosis. There are two studies which may support this dual BBB targeting hypothesis, although with different systems. Liposomes

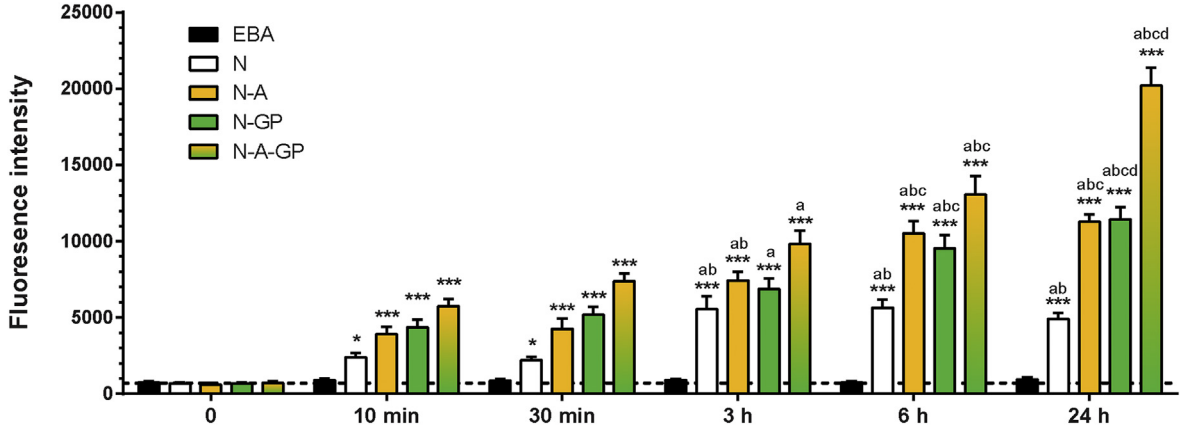

Fig. 11. Fluorescent intensity of EBA in the brain regions of mice after injection of free EBA or EBA encapsulated in non-targeted (N), single- (N-A, N-GP) or dual-targeted (N-A-GP) niosomes measured by optical imaging. Values presented are means ± SD. Statistical analysis: two-way ANOVA, Bonferroni posttest. $*P < 0.5$; $**P < 0.01$; $***P < 0.001$, as compared to the EBA-treated group within each time point; a: as compared to the 10 min, b: as compared to the 30 min, c: as compared to the 3 h, d: as compared to the 6 h time points within each group, $n = 3–4$.

(100 nm) were dually decorated with ligands of the transferrin and LRP receptors expressed at the BBB (Markoutsa et al., 2014). Dual-targeting for BBB receptors increased BBB penetration of NPs both in cultured brain endothelial cells and in mice, indicating that targeting more than one receptors at the BBB can be more effective, similarly to targeting multiple BBB transporters. In another study 2 nm carbon dots prepared by pyrolysis from D-glucose and L-aspartic acid penetrated glioma tissue better than normal brain in mice, but not carbon dots prepared from D-glucose, L-aspartic acid, or D-glucose and L-glutamic acid (Zheng et al., 2015). In this study, however, no experiments were done to reveal the uptake mechanism(s) and whether this was an active, energy dependent process.

Dual-targeted drug delivery systems are also described for other glioma preclinical models, but in these cases not multiple BBB transporters are involved. For example, the ligand of hexose transporters, 2-deoxy-D-glucose, was used as a NP ligand targeting both the BBB and the glioma cells (Jiang et al., 2014). In other systems even if two different ligands are used, only one is specific for the BBB, the other ligand serves for different purposes, like cell penetration. The combination of T7 peptide targeting TfR at the BBB and the cell-penetrating peptide TAT enhanced the efficiency of glioma targeting of liposomes (Zong et al., 2014).

4.3. Mechanism of targeted NP uptake

Modified physiological conditions, such as low temperature or the inhibition of ATP hydrolysis can help to identify the cellular uptake mechanisms of NPs (Fiorentino et al., 2015). In our study the uptake of cargo was decreased in the targeted NP groups by both low temperature and the metabolic inhibitor sodium azide, which is consistent with the hypothesis that the cellular uptake of targeted niosomes was an energy-dependent active process. In agreement with our experiments the uptake of GSH labeled liposomes in brain endothelial cells was also inhibited by low temperature (Maussang et al., 2016).

We also supposed that endocytotic processes might participate in the uptake of targeted niosomes, therefore we used inhibitors of endocytosis, cytochalasin D and filipin. Cytochalasin D is a drug blocking F-actin depolymerization, membrane ruffling and thereby inhibiting macropinocytosis and phagocytosis. Since actin cytoskeleton regulates several endocytotic pathways cytochalasin D is a common inhibitor of endocytosis (Ivanov, 2008). Cytochalasin D pretreatment inhibited the uptake of GSH-PEG liposomes in hCMEC/D3 endothelial cell line (Maussang et al., 2016) as well as the uptake of platelet-derived microparticles (Faille et al., 2012) indicating that the internalization of extracellular NPs into endocytotic vesicles might be an important step in the cellular uptake mecanisms. The antibiotic filipin interacts with cholesterol in the biological membranes and inhibits selectively the lipid raft and caveolae-mediated endocytosis (Ivanov, 2008). Pretreatment of brain endothelial cells with cytochalasin D or filipin significantly decreased the uptake of the cargo in the case of dual-targeted niosomes (N-A-GSH). These data indicate that endocytosis contributes to the cellular uptake of targeted niosomes.

Several specific features of the BBB limit the penetration of drugs to CNS. Intercellular junctions and drug efflux pumps are widely investigated, but the role of the negative surface charge of brain endothelial cells in CNS drug delivery is rather unexplored. This highly negative surface charge is composed of the negatively charged lipids in the cellular plasma membrane and the glycocalyx at the luminal surface. The glycocalyx is a 0.1–1 μm thin layer covering the entire surface of endothelial cells and composed of proteoglycans and glycosaminoglycans (Hervé et al., 2008). The surface charge of cells can be measured by dynamic light scattering (zeta-sizer) and was found to be the most negative in brain endothelial cells among vascular endothelial cells (Ribeiro et al., 2012). This electrostatic barrier may influence the transport of substances and also NPs across the BBB. While NP surface charge was already investigated on BBB integrity and permeability (Fenart et al., 1999; Lockman et al., 2004), the effect of brain endothelial surface charge modification on the permeability of NPs was not measured yet. We modified the highly negative surface charge with neuraminidase and the TMA-DPH cationic lipid. The neuraminidase or sialidase digests the negatively charged sialic acid residues on the luminal surface of vascular endothelial cells and elevates the surface charge of glycocalyx (Born and Palinski, 1985). In our experiments neuraminidase treatment of brain endothelial cells significantly increased the uptake of the cargo of dual-targeted NPs compared with the untargeted and non-treated groups. TMA-DPH elevates the charge of the plasma membrane because it intercalates with the hydrophilic head groups of membrane phospholipids (Ribeiro et al., 2012). TMA-DPH also raised the cellular uptake of cargo in the dual-targeted NP group, similarly to neuraminidase. Our new observations indicate that surface charge at the BBB is important in the uptake mechanism of charged NPs and can be modulated by modification of plasma membrane lipid composition or the glycocalyx.

Surfactants are well known enhancers of absorption and increase drug permeability through the cell membranes or *via* the modulation of intercellular junctions (Deli, 2009). Surfactants are incorporated into the lipid bilayer of cell membranes, and depending on their concentration either change the physical properties and permeability of plasma membranes or result in membrane solubilization leading to cell toxicity (Ujhelyi et al., 2012). Polysorbate surfactants, especially

Solulan C24 which is one of the main components of our niosomes concentration-dependently increased the transepithelial permeability of hidrophilic drug as a result of solubilization of membrane components of Caco-2 cells (Dimitrijevic et al., 2000). We have previously demonstrated that the non-ionic surfactant sugar esters increased the plasma membrane fluidity of epithelial cells which could contribute to the increased transcellular passage of molecules (Kiss et al., 2014). In the present experiments both the non-targeted and dual-targeted niosomes decreased the fluorescent anisotropy in brain endothelial cells, which indicates increased cell membrane fluidity, suggesting the fusion of the nanovesicles with the plasma membrane.

4.4. Possible advantages and limitations of niosomes targeting BBB as a delivery system

Niosomes in terms of stability and permeability for drug-size molecules are comparable to liposomes (Abdelkader et al., 2014; Bartelds et al., 2018). In addition, the components of niosomes are cheap, not sensitive for oxidation, and can be easily stored and handled. Similarly to liposomes, they are suitable for the encapsulation of both water and lipid soluble molecules (Abdelkader et al., 2014). Before our study, the 3.3 kDa hormone, vasoctive intestinal peptide, was the largest cargo encapsulated in niosomes and targeted successfully to brain in mice (Dufes et al., 2004). The molecular mass of our cargo, serum albumin is 20 times bigger, suggesting that niosomes are able to deliver large biomolecules. Due to their non-ionic components and good biodegradability niosomes show low toxicity (Abdelkader et al., 2014). It should be noted, that non-ionic surfactants may increase in a concentration dependent way the plasma membrane fluidity of mammalian cells, as we demonstrated in our previous study with sucrose esters (Kiss et al., 2014), and in our present study with niosomes. This effect may help in the delivery of molecules, but can also contribute to cellular toxicity. While liposomes are already used in pharmacotherapy, only preclinical data, but no clinical studies were reported for niosomes. To assess the efficacy of BBB targeted niosomes as a delivery system, comparative studies including other nanoparticles, like liposomes, and other targeting ligands are needed.

4.5. Conclusion

Ligands targeting brain endothelial transporters elevated the permeability of the albumin cargo across the BBB in the culture model and in mice, and dual-ligand decoration of niosomes was more effective than single ligand labeling. Our data indicate that dual labeling with ligands of multiple SLC transporters can potentially be exploited for BBB targeting of NPs.

Acknowledgements

This work was supported by the Hungarian Scientific Research Fund (OTKA/NKFIH 105622), the National Research, Development and Innovation Office (GINOP-2.2.1-15-2016-00007, GINOP-2.3.2-15-2016-00060) and by the EU-funded Hungarian grant EFOP-3.6.1-16-2016-00008. S.V. was supported by the János Bolyai Research Scholarship of the Hungarian Academy of Sciences (BO/00724/12, BO/00793/18/8). G.P. is a Szent-Györgyi student in the Szeged Scientists Academy Program of the Foundation for the Future of Biomedical Sciences in Szeged implemented with the support of the Ministry of Human Resources (TSZ:34232-3/2016/INTFIN).

References

Abbott, N.J., 2013. Blood-brain barrier structure and function and the challenges for CNS drug delivery. J. Inherit. Metab. Dis. 36, 437–449.
Abbott, N.J., Patabendige, A.A., Dolman, D.E., Yusof, S.R., Begley, D.J., 2010. Structure and function of the blood-brain barrier. Neurobiol. Dis. 37, 13–25.
Abdelkader, H., Alani, A.W., Alany, R.G., 2014. Recent advances in non-ionic surfactant vesicles (niosomes): self-assembly, fabrication, characterization, drug delivery applications and limitations. Drug Deliv. 21, 87–100.
Banks, W.A., 2009. Characteristics of compounds that cross the blood-brain barrier. BMC Neurol. 9 (Suppl. 1), S3.
Bartelds, R., Nematollahi, M.H., Pols, T., Stuart, M.C.A., Pardakhty, A., Asadikaram, G., Poolman, B., 2018. Niosomes, an alternative for liposomal delivery. PLoS One 13, e0194179.
Birngruber, T., Raml, R., Gladdines, W., Gatschelhofer, C., Gander, E., Ghosh, A., Kroath, T., Gaillard, P.J., Pieber, T.R., Sinner, F., 2014. Enhanced doxorubicin delivery to the brain administered through glutathione PEGylated liposomal doxorubicin (2B3-101) as compared with generic Caelyx,(®)/Doxil(®)-a cerebral open flow microperfusion pilot study. J. Pharm. Sci. 103, 1945–1948.
Bocsik, A., Walter, F.R., Gyebrovszki, A., Fülöp, L., Blasig, I., Dabrowski, S., Ötvös, F., Tóth, A., Rákhely, G., Veszelka, S., Vastag, M., Szabó-Révész, P., Deli, M.A., 2016. Reversible opening of intercellular junctions of intestinal epithelial and brain endothelial cells with tight junction modulator peptides. J. Pharm. Sci. 105, 754–765.
Born, G.V., Palinski, W., 1985. Unusually high concentrations of sialic acids on thesurface of vascular endothelia. Br. J. Exp. Pathol. 66, 543–549.
Campos-Bedolla, P., Walter, F.R., Veszelka, S., Deli, M.A., 2014. Role of the blood-brain barrier in the nutrition of the central nervous system. Arch. Med. Res. 45, 610–638.
César-Razquin, A., Snijder, B., Frappier-Brinton, T., 2015. A call for systematic research on solute carriers. Cell 162, 478–487.
Csete, M., Sipos, Á., Kőházi-Kis, A., Szalai, A., Szekeres, G., Matesz, A., Csákó, T., Osvay, K., Bor, Z., Penke, B., Deli, M.A., Veszelka, S., Schmatulla, A., Marti, O., 2007. Comparative study of sub-micrometer polymeric dot-arrays, linear and crossed gratings generated by UV laser based two-beam interference as surfaces for AFM and SPR based bio-sensing. Appl. Surf. Sci. 254, 1194–1205.
Deli, M.A., 2009. Potential use of tight junction modulators to reversibly open membranous barriers and improve drug delivery. Biochim. Biophys. Acta 1788, 892–910.
Deli, M.A., 2011. Drug transport and the blood-brain barrier. In: Tihanyi, K., Vastag, M. (Eds.), Solubility, Delivery, and ADME Problems of Drugs and Drug-Candidates. Bentham Science Publishers Ltd., Washington, pp. 144–165.
Deli, M.A., Abrahám, C.S., Kataoka, Y., Niwa, M., 2005. Permeability studies on in vitro blood-brain barrier models: physiology, pathology, and pharmacology. Cell. Mol. Neurobiol. 25, 59–127.
Dimitrijevic, D., Shaw, A.J., Florence, A.T., 2000. Effects of some non-ionic surfactants on transepithelial permeability in Caco-2 cells. J. Pharm. Pharmacol. 52, 157–162.
Dufes, C., Gaillard, F., Uchegbu, I.F., Schätzlein, A.G., Olivier, J.C., Muller, J.M., 2004. Glucose-targeted niosomes deliver vasoactive intestinal peptide (VIP) to the brain. Int. J. Pharm. 285, 77–85.
Enerson, B.E., Drewes, L.R., 2006. The rat blood-brain barrier transcriptome. J. Cereb. Blood Flow Metab. 26, 959–973.
Faille, D., El-Assaad, F., Mitchell, A.J., Alessi, M.C., Chimini, G., Fusai, T., Grau, G.E., Combes, V., 2012. Endocytosis and intracellular processing of platelet microparticles by brain endothelial cells. J. Cell. Mol. Med. 16, 1731–1738.
Fenart, L., Casanova, A., Dehouck, B., Duhem, C., Slupek, S., Cecchelli, R., Betbeder, D., 1999. Evaluation of effect of charge and lipid coating on ability of 60-nm nanoparticles to cross an in vitro model of the blood-brain barrier. J. Pharmacol. Exp. Ther. 291, 1017–1022.
Fiorentino, I., Gualtieri, R., Barbato, V., Mollo, V., Braun, S., Angrisani, A., Turano, M., Furia, M., Netti, P.A., Guarnieri, D., Fusco, S., Talevi, R., 2015. Energy independent uptake and release of polystyrene nanoparticles in primary mammalian cell cultures. Exp. Cell Res. 330, 240–247.
Gaillard, P.J., 2016. BBB crossing assessment and BBB crossing technologies in CNS drug discovery. Drug Discov. Today Technol. 20, 1–3.
Gaillard, P.J., Appeldoorn, C.C., Dorland, R., van Kregten, J., Manca, F., Vugts, D.J., Windhorst, B., van Dongen, G.A., de Vries, H.E., Maussang, D., van Tellingen, O., 2014. Pharmacokinetics, brain delivery, and efficacy in brain tumor-bearing mice of glutathione pegylated liposomal doxorubicin (2B3-101). PLoS One 1, e82331.
Gromnicova, R., Davies, H.A., Sreekanthreddy, P., Romero, I.A., Lund, T., Roitt, I.M., Phillips, J.B., Male, D.K., 2013. Glucose-coated gold nanoparticles transfer across human brain endothelium and enter astrocytes in vitro. PLoS One 9, e81043.
Grover, A., Hirani, A., Pathak, Y., Sutariya, V., 2014. Brain-targeted delivery of docetaxel by glutathione-coated nanoparticles for brain cancer. AAPS PharmSciTech 15, 1562–1568.
Hervé, F., Ghinea, N., Scherrmann, J.M., 2008. CNS delivery via adsorptive transcytosis. AAPS J. 10, 455–472.
Horvát, S., Fehér, A., Wolburg, H., Sipos, P., Veszelka, S., Tóth, A., Kiss, L., Kurunczi, A., Balogh, G., Kürti, L., Eros, I., Szabó-Révész, P., Deli, M.A., 2009. Sodium hyaluronate as a mucoadhesive component in nasal formulation enhances delivery of molecules to brain tissue. Eur. J. Pharm. Biopharm. 72, 252–259.
Hülper, P., Veszelka, S., Walter, F.R., Wolburg, H., Fallier-Becker, P., Piontek, J., Blasig, I.E., Lakomek, M., Kugler, W., Deli, M.A., 2013. Acute effects of short-chain alkylglycerols on blood-brain barrier properties of cultured brain endothelial cells. Br. J. Pharmacol. 169, 1561–1573.
Ivanov, A.I., 2008. Pharmacological inhibition of endocytic pathways: is it specific enough to be useful? Methods Mol. Biol. 440, 15–33.
Jiang, X., Xin, H., Ren, Q., Gu, J., Zhu, L., Du, F., Feng, C., Xie, Y., Sha, X., Fang, X., 2014. Nanoparticles of 2-deoxy-D-glucose functionalized poly(ethylene glycol)-co-poly (trimethylene carbonate) for dual-targeted drug delivery in glioma treatment. Biomaterials 35, 518–529.
Johnsen, K.B., Moos, T., 2016. Revisiting nanoparticle technology for blood-brain barrier transport: unfolding at the endothelial gate improves the fate of transferrin receptor-targeted liposomes. J. Control. Release 28, 32–46.
Keren, S., Gheysens, O., Levin, C.S., Gambhir, S.S., 2008. A comparison between a time

domain and continuous wave small animal optical imaging system. IEEE Trans. Med. Imaging 27, 58–63.
Kiss, L., Walter, F.R., Bocsik, A., Veszelka, S., Ozsvári, B., Puskás, L.G., Szabó-Révész, P., Deli, M.A., 2013. Kinetic analysis of the toxicity of pharmaceutical excipients Cremophor EL and RH40 on endothelial and epithelial cells. J. Pharm. Sci. 102, 1173–1181.
Kiss, L., Hellinger, É., Pilbat, A.M., Kittel, Á., Török, Z., Füredi, A., Szakács, G., Veszelka, S., Sipos, P., Ózsvári, B., Puskás, L.G., Vastag, M., Szabó-Révész, P., Deli, M.A., 2014. Sucrose esters increase drug penetration, but do not inhibit P-glycoprotein in Caco-2 intestinal epithelial cells. J. Pharm. Sci. 103, 3107–3119.
Kreuter, J., 2014. Drug delivery to the central nervous system by polymeric nanoparticles: what do we know? Adv. Drug Deliv. Rev. 71, 2–14.
Kumar, A.T.N., Raymond, S.B., Dunn, A.K., Bacskai, B.J., Boas, D.A., 2008. A time domain fluorescence tomography system for small animal imaging. IEEE Trans. Med. Imaging 27, 1152–1163.
Lénárt, N., Walter, F.R., Bocsik, A., Sántha, P., Tóth, M.E., Harazin, A., Tóth, A.E., Vizler, C., Török, Z., Pilbat, A.M., Vígh, L., Puskás, L.G., Sántha, M., Deli, M.A., 2015. Cultured Cells of the Blood-Brain Barrier From Apolipoprotein B-100 Transgenic Mice: Effects of Oxidized Low-Density Lipoprotein Treatment. Fluids Barriers CNS.17. pp. 12–17.
Lindqvist, A., Rip, J., van Kregten, J., Gaillard, P.J., Hammarlund-Udenaes, M., 2016. In vivo functional evaluation of increased brain delivery of the opioid peptide DAMGO by glutathione-PEGylated liposomes. Pharm. Res. 33, 177–185.
Liu, D., Li, Y., Deng, J., Yang, W., 2014. Helix-sense-selective polymerization of achiral substituted acetylene in chiral micelles for preparing optically active polymer nanoparticles: effects of chiral emulsifiers. Polymer 55, 840–847.
Livak, K.J., Schmittgen, T.D., 2001. Analysis of relative gene expression data using real-time quantitative PCR and the 2(−Delta Delta C(T)) method. Methods 25, 402–408.
Lockman, P.R., Koziara, J.M., Mumper, R.J., Allen, D.D., 2004. Nanoparticle surface charges alter blood-brain barrier integrity and permeability. J. Drug Target. 12, 635–641.
Loureiro, J.A., Gomes, B., Fricker, G., Cardoso, I., Ribeiro, C.A., Gaiteiro, C., Coelho, M.A., Pereira, Mdo C., Rocha, S., 2015. Dual ligand immunoliposomes for drug delivery to the brain. Colloids Surf. B. Biointerfaces. 134, 213–219.
Markoutsa, E., Papadia, K., Giannou, A.D., Spella, M., Cagnotto, A., Salmona, M., Stathopoulos, G.T., Antimisiaris, S.G., 2014. Mono and dually decorated nanoliposomes for brain targeting, in vitro and in vivo studies. Pharm. Res. 31, 1275–1289.
Masserini, M., 2013. Nanoparticles for brain drug delivery. ISRN. Biochem. 2013, 238428.
Maussang, D., Rip, J., van Kregten, J., van den Heuvel, A., van der Pol, S., van der Boom, B., Reijerkerk, A., Chen, L., de Boer, M., Gaillard, P., de Vries, H., 2016. Glutathione conjugation dose-dependently increases brain-specific liposomal drug delivery in vitro and in vivo. Drug Discov. Today Technol. 20, 59–69.
Nakagawa, S., Deli, M.A., Kawaguchi, H., Shimizudani, T., Shimono, T., Kittel, A., Tanaka, K., Niwa, M., 2009. A new blood-brain barrier model using primary rat brain endothelial cells, pericytes and astrocytes. Neurochem. Int. 54, 253–263.
Pardridge, W.M., 2012. Drug transport across the blood-brain barrier. J. Cereb. Blood Flow Metab. 11, 1959–1972.
Pardridge, W.M., 2015. Targeted delivery of protein and gene medicines through the blood-brain barrier. Clin. Pharmacol. Ther. 97, 347–361.
Pardridge, W.M., 2016. CSF, blood-brain barrier, and brain drug delivery. Expert. Opin. Drug. Deliv. 13, 963–975.
Patching, S.G., 2017. Glucose transporters at the blood-brain barrier: function, regulation and gateways for drug delivery. Mol. Neurobiol. 54, 1046–1077.
Perrière, N., Demeuse, P., Garcia, E., Regina, A., Debray, M., Andreux, J.P., Couvreur, P., Scherrmann, J.M., Temsamani, J., Couraud, P.O., Deli, M.A., Roux, F., 2005. Puromycin-based purification of rat brain capillary endothelial cell cultures. Effect on the expression of blood-brain barrier-specific properties. J. Neurochem. 93, 279–289.
Rask-Andersen, M., Masuram, S., Fredriksson, R., Schiöth, H.B., 2013. Solute carriers as drug targets: current use, clinical trials and prospective. Mol. Asp. Med. 34, 702–710.
Ribeiro, M.M., Domingues, M.M., Freire, J.M., Santos, N.C., Castanho, M.A., 2012. Translocating the blood-brain barrier using electrostatics. Front. Cell. Neurosci. 11, 6–44.
Rip, J., Chen, L., Hartman, R., van den Heuvel, A., Reijerkerk, A., van Kregten, J., van der Boom, B., Appeldoorn, C., de Boer, M., Maussang, D., de Lange, E.C., Gaillard, P.J., 2014. Glutathione PEGylated liposomes: pharmacokinetics and delivery of cargo across the blood-brain barrier in rats. J. Drug Target. 22, 460–467.
Saraiva, C., Praça, C., Ferreira, R., Santos, T., Ferreira, L., Bernardino, L., 2016. Nanoparticle-mediated brain drug delivery: overcoming blood-brain barrier to treat neurodegenerative diseases. J. Control. Release 10, 34–47.
Shawahna, R., Uchida, Y., Declèves, X., Ohtsuki, S., Yousif, S., Dauchy, S., Jacob, A., Chassoux, F., Daumas-Duport, C., Couraud, P.O., Terasaki, T., Scherrmann, J.M., 2011. Transcriptomic and quantitative proteomic analysis of transporters and drug metabolizing enzymes in freshly isolated human brain microvessels. Mol. Pharm. 8, 1332–1341.
Singh, A., Satchell, S.C., Neal, C.R., McKenzie, E.A., Tooke, J.E., Mathieson, P.W., 2007. Glomerular endothelial glycocalyx constitutes a barrier to protein permeability. J. Am. Soc. Nephrol. 18, 2885–2893.
Sipos, E., Kurunczi, A., Fehér, A., Penke, Z., Fülöp, L., Kasza, A., Horváth, J., Horvát, S., Veszelka, S., Balogh, G., Kürti, L., Eros, I., Szabó-Révész, P., Párducz, A., Penke, B., Deli, M.A., 2010. Intranasal delivery of human beta-amyloid peptide in rats: effective brain targeting. Cell. Mol. Neurobiol. 30, 405–413.
Tóth, A.E., Tóth, A., Walter, F.R., Kiss, L., Veszelka, S., Ózsvári, B., Puskás, L.G., Heimesaat, M.M., Dohgu, S., Kataoka, Y., Rákhely, G., Deli, M.A., 2014. Compounds blocking methylglyoxal-induced protein modification and brain endothelial injury. Arch. Med. Res. 45, 753–764.
Uchida, Y., Ito, K., Ohtsuki, S., Kubo, Y., Suzuki, T., Terasaki, T., 2015. Major involvement of Na(+) -dependent multivitamin transporter (SLC5A6/SMVT) in uptake of biotin and pantothenic acid by human brain capillary endothelial cells. J. Neurochem. 134, 97–112.
Ujhelyi, Z., Fenyvesi, F., Váradi, J., Fehér, P., Kiss, T., Veszelka, S., Deli, M., Vecsernyés, M., Bácskay, I., 2012. Evaluation of cytotoxicity of surfactants used in self-micro emulsifying drug delivery systems and their effects on paracellular transport in Caco-2 cell monolayer. Eur. J. Pharm. Sci. 47, 564–573.
Uyama, O., Okamura, N., Yanase, M., Narita, M., Kawabata, K., Sugita, M., 1988. Quantitative evaluation of vascular permeability in the gerbil brain after transient ischemia using Evans blue fluorescence. J. Cereb. Blood Flow Metab. 8, 282–284.
Veszelka, S., Urbányi, Z., Pázmány, T., Németh, L., Obál, I., Dung, N.T., Abrahám, C.S., Szabó, G., Deli, M.A., 2003. Human serum amyloid P component attenuates the bacterial lipopolysaccharide-induced increase in blood-brain barrier permeability in mice. Neurosci. Lett. 352, 57–60.
Veszelka, S., Pásztói, M., Farkas, A.E., Krizbai, I., Ngo, T.K., Niwa, M., Ábrahám, C.S., Deli, M.A., 2007. Pentosan polysulfate protects brain endothelial cells against bacterial lipopolysaccharide-induced damages. Neurochem. Int. 50, 219–228.
Veszelka, S., Meszaros, M., Kiss, L., Kota, Z., Pali, T., Hoyk, Z., Bozso, Z., Fulop, L., Toth, A., Rakhely, G., Deli, M.A., 2017. Biotin and glutathione targeting of solid nanoparticles to cross human brain endothelial cells. Curr. Pharm. Des. 23, 4198–4205.
Veszelka, S., Tóth, A., Walter, F.R., Tóth, A.E., Gróf, I., Mészáros, M., Bocsik, A., Hellinger, É., Vastag, M., Rákhely, G., Deli, M.A., 2018. Comparison of a rat primary cell-based blood-brain barrier model with epithelial and brain endothelial cell lines: gene expression and drug transport. Front. Mol. Neurosci. 11, 166.
Walter, F.R., Veszelka, S., Pásztói, M., Péterfi, Z.A., Tóth, A., Rákhely, G., Cervenak, L., Ábrahám, C.S., Deli, M.A., 2015. Tesmilifene modifies brain endothelial functions and opens the blood-brain/blood-glioma barrier. J. Neurochem. 134, 1040–1054.
Wohlfart, S., Gelperina, S., Kreuter, J., 2012. Transport of drugs across the blood-brain barrier by nanoparticles. J. Control. Release 161, 264–273.
Zheng, M., Ruan, S., Liu, S., Sun, T., Qu, D., Zhao, H., Xie, Z., Gao, H., Jing, X., Sun, Z., 2015. Self-targeting fluorescent carbon dots for diagnosis of brain cancer cells. ACS Nano 9, 11455–11461.
Zhou, Y., Peng, Z., Seven, E.S., Leblanc, R.M., 2018. Crossing the blood-brain barrier with nanoparticles. J. Control. Release 28, 290–303.
Zong, T., Mei, L., Gao, H., Shi, K., Chen, J., Wang, Y., Zhang, Q., Yang, Y., He, Q., 2014. Enhanced glioma targeting and penetration by dual-targeting liposome co-modified with T7 and TAT. J. Pharm. Sci. 103, 3891–3901.